

Adopting a human developmental visual diet yields robust, shape-based AI vision

Zejin Lu^{*1,2}, Sushrut Thorat^{*1}, Radoslaw M Cichy², & Tim C Kietzmann⁺¹

¹ Machine Learning Group, Institute for Cognitive Science, Osnabrück University, Osnabrück, Germany.

² Neural Dynamics of Visual Cognition Group, Department of Education and Psychology, Freie Universität Berlin, Berlin, Germany.

* Shared first authorship.

+ Corresponding author

Summary

Despite years of research and the dramatic scaling of artificial intelligence (AI) systems, a striking misalignment between artificial and human vision persists. Contrary to humans, AI heavily relies on texture-features rather than shape information¹⁻³, lacks robustness to image distortions⁴, remains highly vulnerable to adversarial attacks⁵⁻⁷, and struggles to recognise simple abstract shapes within complex backgrounds⁸. To close this gap, we here introduce a solution that arises from a previously underexplored direction: rather than scaling up, we take inspiration from how human vision develops from early infancy into adulthood. We quantified the visual maturation by synthesising decades of psychophysical and neurophysiological research into a novel developmental visual diet (DVD) for AI vision. We show that guiding AI systems through this human-inspired curriculum produces models that closely align with human behaviour on every hallmark of robust vision tested yielding the strongest reported reliance on shape information to date, abstract shape recognition beyond the state of the art, higher robustness to image corruptions, and stronger resilience to adversarial attacks. By outperforming high parameter AI foundation models trained on orders of magnitude more data, we provide evidence that robust AI vision can be achieved by guiding the way how a model learns, not merely how much it learns, offering a resource-efficient route toward safer and more human-like artificial visual systems.

Main

Despite the unprecedented scale and capabilities of contemporary AI vision systems, human vision remains far superior, most prominently in terms of its robustness. Unlike humans, AI vision continues to rely on texture-based rather than shape-based features¹⁻³, has poor generalisation to image degradations⁴, is often unable to recognise abstract shapes⁸, and suffers from adversarial attacks⁵⁻⁷. Thus, despite advances in the capabilities of AI systems, human and artificial vision remain fundamentally misaligned. This constitutes an important roadblock in the development of reliable, robust, and efficient AI.

Here we hypothesise that the key to human-level visual robustness lies in overcoming the fundamental differences in visual upbringing between humans and AI systems. While AI systems are trained with high-fidelity input throughout their training trajectory, human visual development is, initially, severely limited in visual acuity, chromatic sensitivity and contrast sensitivity. Early evidence for the functional importance of a gradual visual development can be found in both neuroscience

and AI. For example, children whose congenital cataracts are removed can nevertheless exhibit lasting recognition deficits⁹, likely due to missing parts of the slow developmental trajectory of healthy controls. Accordingly, AI systems that involve training with single or multiple fixed blurring stages were shown to be more robust¹⁰⁻¹³, albeit remaining far from human-level reliability.

To test our hypothesis, we reviewed the existing psychophysical evidence on how human vision develops from newborn to 25 years of age and synthesised the developmental trajectories of three core dimensions of visual maturation (visual acuity, chromatic sensitivity, and contrast sensitivity) into a preprocessing pipeline for AI vision. Across a series of experiments, we demonstrate that guiding AI through this human developmental visual diet (DVD), instead of the gold standard of high-res AI vision training, is a highly effective and reliable means to approaching human-level robustness in visual inference. Deep neural networks (DNNs) trained with DVD exhibit shape bias beyond the state of the art, greater reliance on spatial integration of visual features, increased capability of abstract shape recognition, as well as heightened resilience to image degradations and adversarial attacks.

Results

In our experiments, we contrasted DNNs trained on high-res images (gold standard) with networks trained with DVD, a developmental trajectory set up so that the full model training corresponds to 25 years of human visual development. Various model architectures were trained with an object categorization objective across multiple image datasets, including mini-ecose⁵⁴, ecose¹³ or ImageNet 1K¹⁴. Subsequent to training, the models were evaluated across a test battery for inferential robustness (Fig. 1A), comparing models to human behavioural data where available.

The mapping from chronological months to training epochs was handled by the hyperparameter α . For the development of visual acuity, we mapped the Snellen-equivalent terms onto a Gaussian blur parameter (σ , Fig 1B; see Methods). Contrast sensitivity trajectories were converted into a frequency-domain threshold modulation (Fig. 1C; see Methods), controlled by hyperparameters β (initial threshold) and λ (sensitivity mapping). Chromatic sensitivity was implemented via adjustments in colour fidelity (Fig. 1D; see Methods). By exploring the three hyperparameters of DVD (α , β , λ), we modulated the extent and intensity of early visual experiences the model receives during training (see Fig. 1E for example trajectories). Irrespective of model training setup or training age, all testing was performed on the same high-res test images.

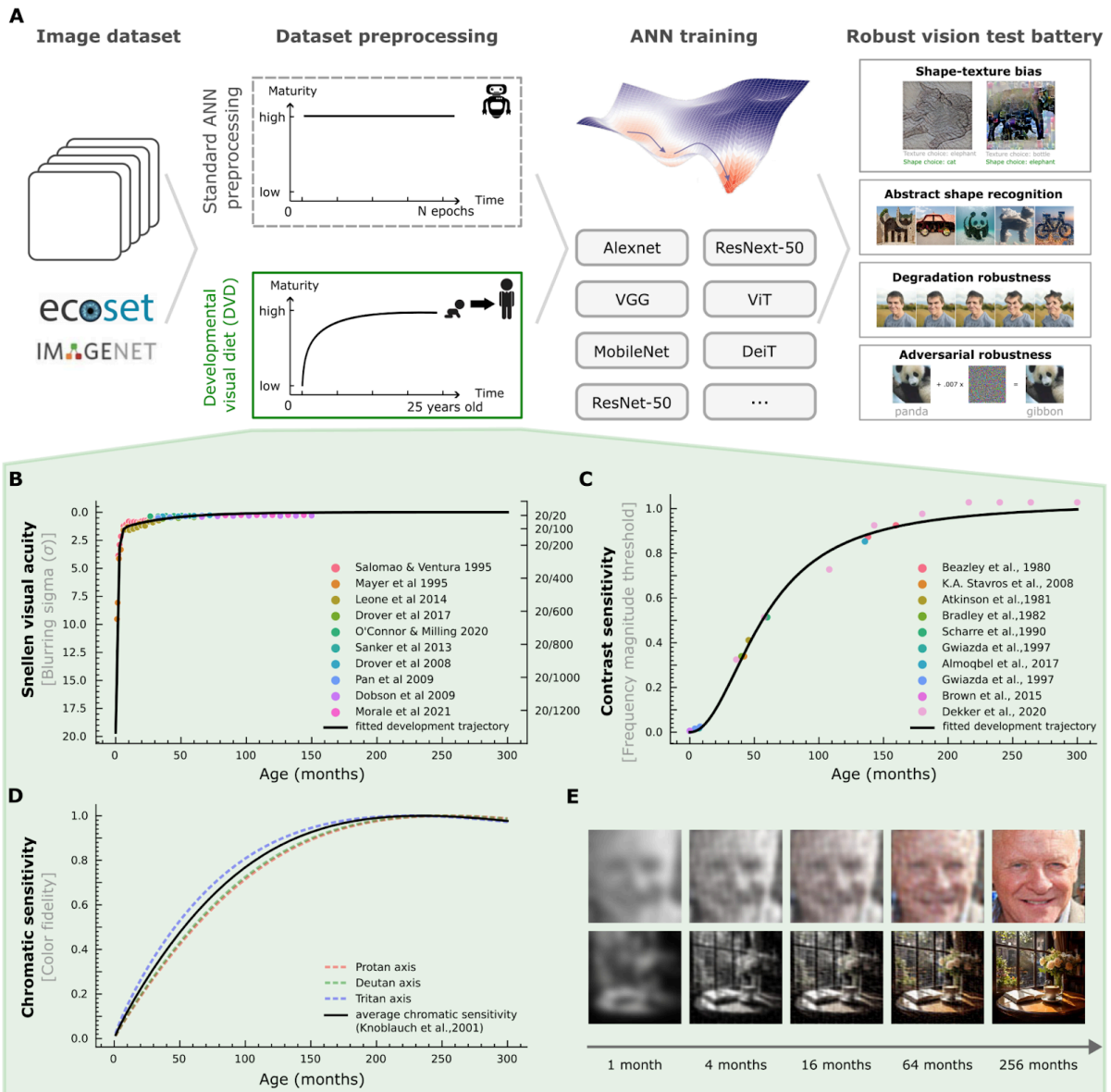


Figure 1 | Following the developmental trajectory of visual acuity, chromatic sensitivity, and contrast sensitivity from newborn to 25-year-old, as an effective means of training robust AI vision systems. A. Schematic of our training and analysis pipeline for comprehensively evaluating Developmental Visual Diet (DVD) vs standard training regimes for artificial neural networks (ANNs). B-D. Developmental trajectories of the three aspects of vision modelled by DVD, as synthesised from a multitude of psychophysical experiments across age groups. E. DVD example images at selected developmental stages, illustrating the progression of visual experience from newborns to adults.

DVD training promotes near-human levels of shape bias

A defining feature of human visual perception is that, when presented with object images for which the texture and shape information are in conflict (Fig. 2A), observers reliably report perceiving the object category in line with the shape information (shape over texture preference is around 0.96 (96%) in adults¹ and 0.90 (90%) in 4-year-olds¹⁵). By contrast, DNNs, irrespective of network architecture, training dataset, dataset size, or training objective, exhibit a strong tendency towards

texture-based decisions (their shape bias scores typically fall in the 0.2-0.4 range^{1,16}). The texture-preference in DNNs therefore constitutes a signature difference to human vision.

We first explored the effect of DVD on the shape/texture bias in ANNs by performing a comprehensive hyperparameter sweep of DVD based on the ResNet-50 model architecture¹⁷, trained on a smaller-scale image-dataset (mini-ecoset¹³, 280k images, for training details see Methods, Fig. 2B). Observing a tradeoff between shape-selectivity and accuracy across hyperparameter settings, three representative model configurations were chosen for subsequent analyses: shape-bias favoured (DVD-S; 0.94 shape bias, aligning closely with the human range of 0.90-0.97), recognition performance favoured (DVD-P; increased shape bias from 0.32 (baseline) to 0.73 while getting similar overall accuracy to baseline model), and striking a balance between the two (DVD-B; 0.82 shape bias with a modest accuracy loss of approximately 4.9% compared to gold-standard training with high-res images). Crucially, when scaling these 3 variants to full ecoset¹³ training (1.5 million images, 565 basic-level categories), the prior results were closely reproduced (Fig. 2B, right). While the control model achieved a shape bias of 0.34 at 62.99% accuracy, DVD-S delivered a shape bias of 0.90, i.e. within the human range; DVD-P exhibited a shape bias of 0.70, alongside a slight accuracy increase compared to baseline (from 62.99% to 65.03%); and DVD-B delivered a shape bias of 0.83, close to the human range, at a marginal 4.3 percentage-point accuracy decline over baseline. Thus, DVD training provided an increase in shape-selectivity by 105.88% (DVD-P), 141.18% (DVD-B) and 164.71% (DVD-S) over our gold-standard baseline with high-res training. A category-specific depiction of shape bias for DVD-P, the ResNet-50 baseline, and human observers is provided as a supplement (Fig. S1) alongside illustrative examples showing shape/texture behaviour for DVD, ResNet-50 baseline, and ChatGPT4o.

Importantly, the shape-bias observed in our DVD-trained ResNet-50 model not only outperforms the corresponding control models by a large margin, but also all other contemporary ANN models tested (Fig. 2C), setting the new state-of-the-art in shape-selectivity and closing the gap to the human range of shape-selectivity. These included standard supervised convolutional neural networks (CNNs), vision transformers (ViTs)^{18,19}, self-supervised models, and multimodal vision-language models. Note that these models include DNNs trained on orders of magnitude more data, as well as models operating at orders of magnitude more model parameters, highlighting the effectiveness of DVD training, even in smaller-scale data/model scenarios.

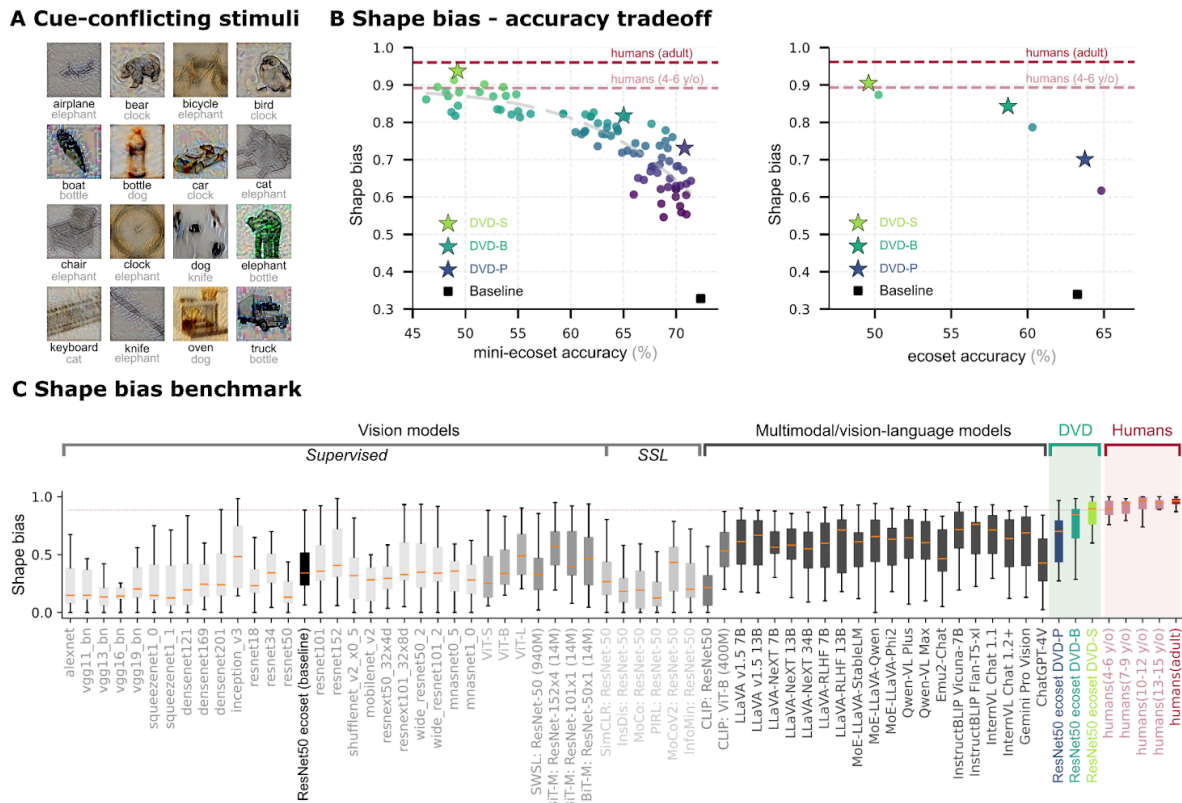
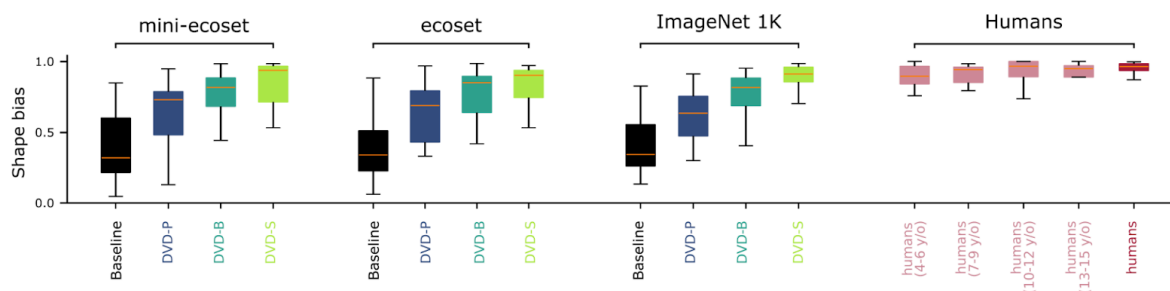


Figure 2 | Models trained with DVD close the gap to human-level shape bias. **A.** Example cue-conflict stimuli from the 16 object categories tested. Shape and texture cues are intentionally mismatched (e.g., an object with the shape of an airplane is shown with the texture of elephant skin), to test which of the two feature types underlies human and AI decisions. Shape categories are indicated in black, texture categories in grey. **B.** Trade-off between object recognition accuracy and shape bias across models trained on mini-ecosest (0.28 million images) and full ecosest (1.5 million images). Three exemplary DVD-trained models were selected for subsequent analyses: a high recognition performance variant (DVD-P); and a balanced variant (DVD-B), which achieves close to human-level shape bias while incurring only a modest cost in accuracy; and a model prioritising shape-based decision making (DVD-S). **C.** Comparison of shape bias between DVD models, standard supervised/self-supervised vision models, large-scale multimodal vision-language models (VLMs) and humans across different age groups. Boxplots show category-dependent distribution of shape/texture biases (shape bias: high values, texture bias: low values), midline represents the median, bounds indicate the 25th and 75th percentiles, and whiskers extend to the 5th and 95th percentiles. The dotted line indicates the lower bound of average human-level shape bias (88% average shape-based decisions of 4-6-year-old humans).

The generality of our results was ensured by a sequence of additional experiments. First, we expanded training from mini-ecosest, and ecosest to also include ImageNet-1k¹⁴ training. Across all three datasets, DVD consistently increased shape bias compared to the baseline, with shape bias progressively rising from DVD-P to DVD-B to DVD-S. DVD-S achieved shape bias close to human levels regardless of the dataset (Fig. 3A). Second, in addition to ResNet-50 training, we included 8 further contemporary ANN architectures, including various convolutional and ViT models, all trained according to the DVD-B scheme (Fig. 3B). In every case, DVD-B preprocessing substantially increased

shape bias, confirming the broad effectiveness of the method in promoting shape-based representations across model types.

A Generalisation across datasets



B Generalisation across models trained on ecocet

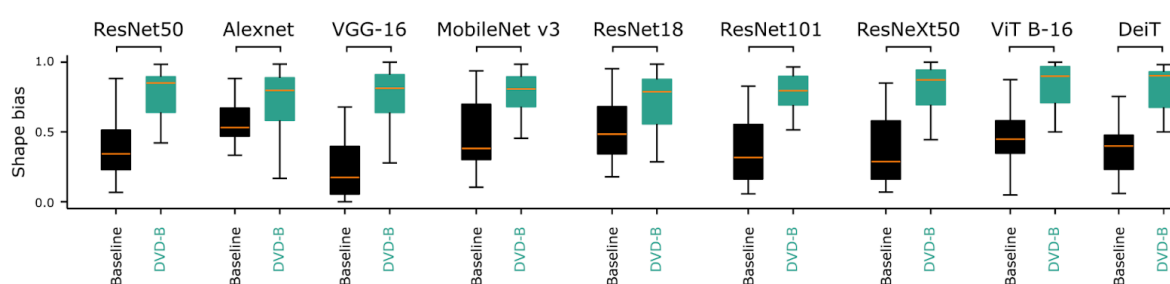


Figure 3 | Results generalisation across vision datasets and ANN architectures. A. Generalisation of results across training datasets (0.28 million mini-ecocet, 1.50 million ecocet and 1.28 million ImageNet 1k). **B.** Generalisation of results across a range of DNN architectures, including both CNNs and ViTs.

We quantified the emergence of shape bias over time by analysing the DVD-B networks across training epochs as they progressed through the developmental trajectory (in line with training, 2 months of human development equate to 1 training epoch). We observe a strong shape bias very early in training, which remained relatively stable as learning progressed (0.87 shape bias at an early stage corresponding to ~20 months of age, Fig. 4A and Fig. S2), akin to psychophysical evidence that human infants are already shape-biased by around two years of age²⁰. In contrast, the baseline ResNet-50 model remained consistently texture-biased across training (average shape bias ~0.43).

Next, we explored how DVD affects the decision-making strategies of our models - a key step in linking training regime to classification behaviour. Layer-Wise Relevance Propagation (LRP; see Methods), run across the cue-conflict stimuli, revealed that our DVD-trained model predominantly relied on shape-related features, whereas the baseline ResNet-50 model assigned greater importance to local features or highly distributed texture patches (Fig. 4B; see Methods for analysis details). A stronger focus on shape-related features, rather than local textures or texture patches, indicates a perceptual strategy more aligned with human visual decision making.

To understand the impact of each of the three developmental aspects, acuity, contrast, and colour, we performed controlled rearing experiments, which systematically tested all seven combinations for their impact on shape bias. This systematic manipulation revealed, in contrast to the previous focus on blur in the literature, a central role of contrast sensitivity development as a key driver of shape bias in our models. Models trained with contrast sensitivity development achieved a shape bias of

0.73 (compared to 0.85 observed for the original DVD-B model (Fig. 2C, Fig. S3)). In contrast, models exposed only to visual acuity development, or to both visual acuity and chromatic sensitivity development, exhibited far smaller increases in shape bias (0.41 and 0.44, respectively), relative to the baseline shape bias of 0.34.

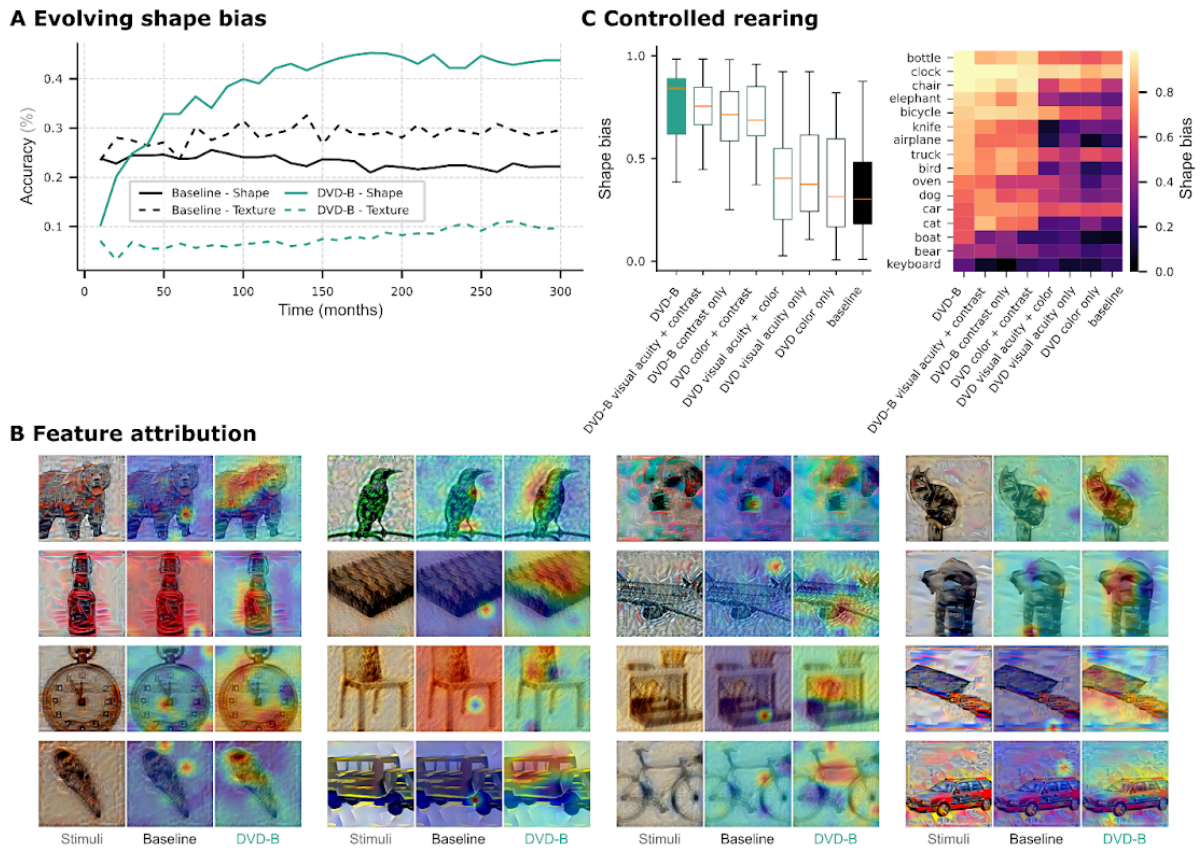


Figure 4 | In-depth investigation of the emergence of shape bias in ANNs and the underlying feature selectivity. **A.** Evolving shape bias in the DVD-B model from birth to 25 years old (300 months; 2 months/epoch for DVD-B; see also Fig. S2), as reflected by a rising proportion of shape-based choices on cue-conflict trials (i.e., predictions matching the shape category). In contrast, the baseline model exhibits a consistent preference for texture-based choices. **B.** Feature importance visualisation using layer-wise relevance propagation, indicating that DVD-B relies more strongly on image regions corresponding to the object in question (see also Fig. S4). **C.** Controlled rearing experiments to study the role of different visual aspects in development (based on DVD-B) indicate a strong impact of contrast sensitivity development. Including all 3 aspects of visual development yields the most consistent shape bias across categories.

Together, our results indicate that taking inspiration from the human developmental visual diet is a highly effective way to bias AI vision systems towards more human-like perceptual decision making, delivering the new state-of-the-art in shape bias across a large range of open-source and closed-source models, including AI foundation models.

DVD-trained models exhibit higher recall for abstract shapes embedded in complex contexts

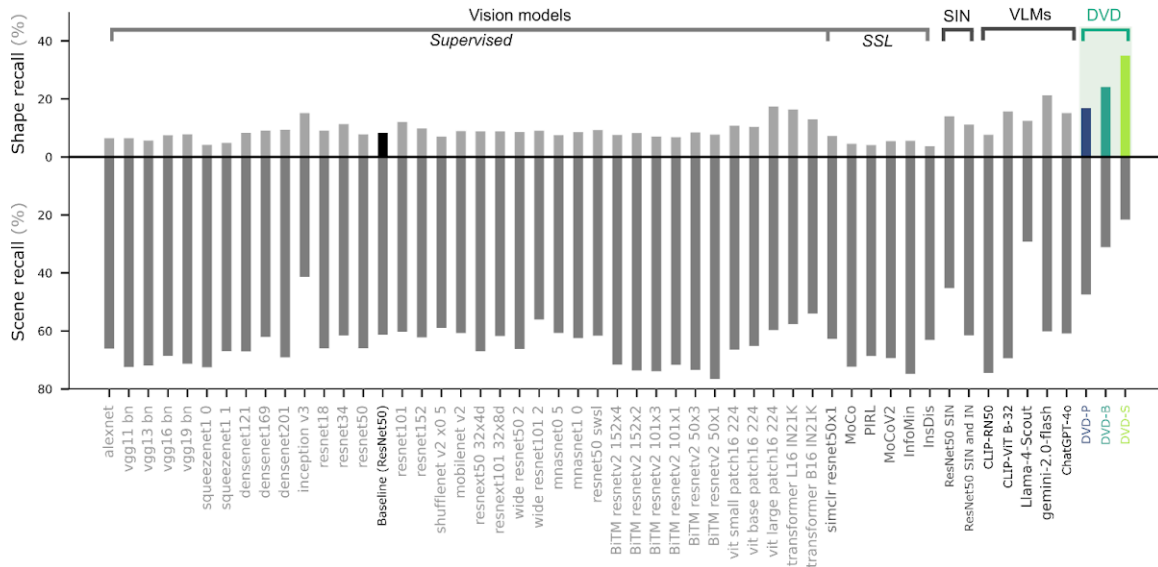
Additional evidence for the misalignment between human and AI vision comes from experiments on abstract shapes⁸. Humans effortlessly recognize abstract shapes, i.e. recognizable forms defined by their overall configuration rather than specific textures or colors, even when embedded within complex natural scenes (Fig. 5A). In contrast, current AI systems, including large-scale vision-language models (VLMs), struggle to detect such shapes, and instead rely on scene-based cues⁸.

To assess the efficacy of DVD in enhancing abstract shape recognition within naturalistic contexts, we evaluated DVD-trained models alongside gold-standard baseline models and a large array of DNN architectures using the IllusionBench dataset - a benchmark that specifically tests shape recognition through scene-embedded visual arrangements (6874 images, 16 shapes, 11 background scenes, see Methods). In this benchmark, shape recall reflects a model's tendency to make predictions based on abstract shape cues, while scene recall reflects its tendency to rely on background scene or texture cues. Conventional CNN models, such the baseline ResNet50, achieved a shape recall of 8.71%. The best-performing Vision Transformer (ViT-L) reached 17.13%. Large-scale VLMs, including CLIP-RN50 and CLIP-ViT B-32, attained 16.72% and 15.45%, respectively, and ResNet50 trained on a style-transferred dataset reached 14.32%. In contrast, our DVD-trained ResNet-50 (DVD-S, trained on ImageNet 1k) significantly outperformed all other tested models, including latest AI foundation models, by achieving a shape recall rate of 36.21% (Fig. 5B). Notably, large-scale AI foundation models, even though explicitly prompted to spot the shape in the background, were outperformed (shape recall for Llama-4-Scout (12.47%), Gemini-2.0-flash (21.24%), and ChatGPT 4o (15.17%)). This again demonstrates the ability of DVD training to achieve more human-aligned representations even when operating at orders of magnitude less data and model parameters. DVD-S models also displayed substantially lower reliance on scene cues (20.07% scene recall) compared to approximately 60% scene recall rates in other models. Shape recall improved systematically across the DVD family as the strength of early visual developmental constraints increased, from 16.43% in DVD-P to 36.21% in DVD-S, while texture-based recall declined (from 46.32% to 20.07%). Further analyses of the internal representations of the various models revealed a striking pattern that differentiates DVD-trained models from other models. Visualising model embeddings of IllusionBench stimuli using t-SNE²¹ (Fig. 5C), we observe that only DVD-trained models distinctly clustered images by abstract shape category, whereas baseline ResNet50, CLIP-ViT B-32, as well as ResNet50 style-transferred models predominantly clustered images based on scene context. Together, these analyses demonstrate that DVD training substantially alters the visual features learned to perform the task, promoting the spatial integration of distributed shape cues.

A Examples of abstract shapes hidden in scenes



B Shape recall vs. scene recall benchmark



C t-SNE visualisation distinguishing abstract shapes from scenes

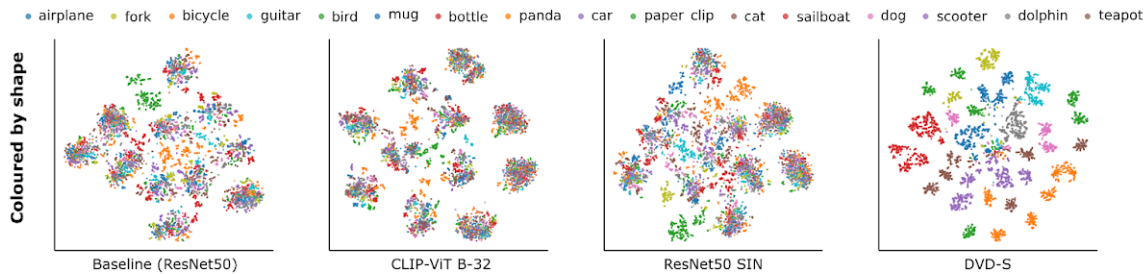


Figure 5 | Models trained with DVD exhibit enhanced recognition of abstract shapes hidden within complex scenes. **A.** Example IllusionBench stimuli of abstract shapes hidden in scene contexts. **B.** Shape recall vs. scene recall benchmark for DVD-trained models, as well as a large range of control models, including AI foundation models and large-scale multimodal vision-language models. **C.** t-SNE embeddings of IllusionBench images, colour coded by object category. Only DVD-trained models cluster images according to their abstract shape categories, whereas other models predominantly cluster images based on their scene contexts (also see Fig. S5).

DVD training enhances robustness to various types of image degradation

Having established the reliance on spatially-integrative shape-like decisions in DVD-trained DNNs, we tested the models for their behavioural robustness in the face of degraded input⁴ - a hallmark of our robust human vision. Cases of image blur, image noise, quality deficits, as well as environmental factors such as rain and snow, were considered. While human performance is highly robust, and

degrades gracefully across severity levels, prior tests of AI vision models revealed a dramatic drop in performance even at low levels of image degradation.

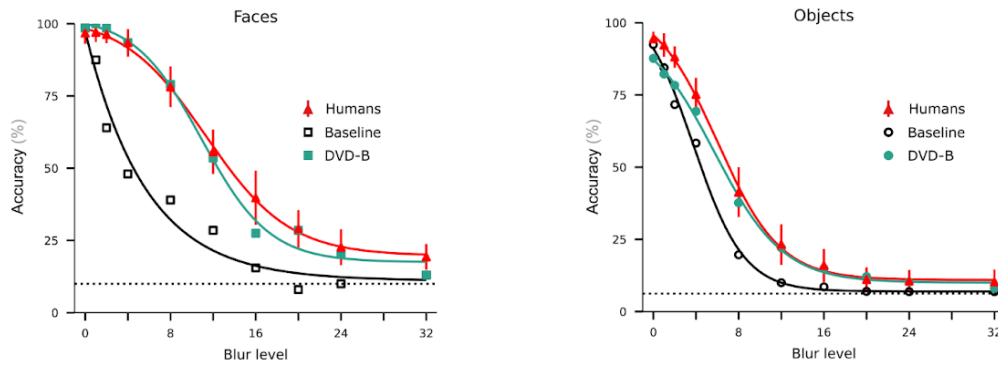
To examine whether DVD is able to close the gap between biological and artificial vision, we first compared a trained DVD-B model with a baseline ResNet50 under increasing levels of Gaussian blur applied to images depicting objects and faces (see Methods). Blur is a particularly challenging degradation because it directly disrupts the fine spatial details and edges that many artificial vision systems rely on for recognition, while human recognition abilities degrade gracefully⁹. This makes blur an important test case for evaluating whether a model has learned to rely, akin to humans, on global, integrative information rather than relying on local detail. As blur severity increases, the baseline model shows a sharp drop in recognition accuracy, while the DVD-trained model maintains significantly higher accuracy, approximately following human behavioural data (Fig. 6A; human data from Jang et al., 2021⁹).

We then evaluated baseline and DVD-trained models across 16 additional types of degradations (4 types of noise, 4 types of blur, 4 types of weather disruption, 4 types of image quality deficits, Fig. 6B; see Methods), each at 5 severity levels from mild (1) to strong (5). At high severities, DVD accuracy was 2 times higher than baseline models for noise, blur, and challenging weather effects, and 3-4 times higher for image quality deficits. These results demonstrate that DVD training greatly improves robustness under challenging conditions.

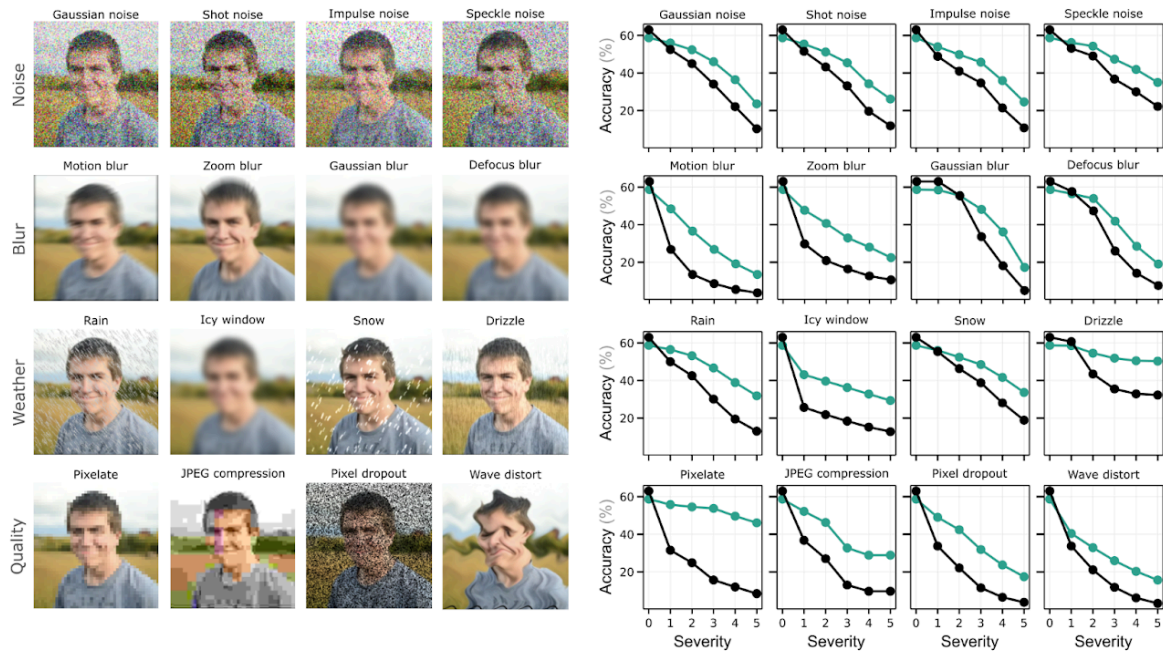
DVD training enhances robustness to white- and black-box adversarial attacks

Adversarial attacks, i.e. small, but targeted image perturbations can dramatically bias and impair model performance⁵⁻⁷. While often imperceptible for humans, these attacks pose yet another major challenge for AI vision systems and showcase the problems in terms of behavioural alignment. We tested whether DVD training improves adversarial robustness, again compared to control models trained with the same architecture, training-dataset and task, but following the gold-standard of high-res training. DVD-trained models exhibit marked improvements under both black-box²² (Fig. 7A) as well as white-box²³ (Fig. 7B) adversarial attacks. From the family of black-box attacks, a DVD-trained model achieves about 80% higher accuracy for L2-based Gaussian and uniform noise at severity 5, and about 3 times higher accuracy under salt-and-pepper noise at the same severity. Against white-box attacks, DVD improves performance against Fast Gradient Sign Method (FGSM⁵; from 8% to 40%), against the Fast Gradient Method (FGM⁵; from 12% to 33%), and against a Projected Gradient Descent attack (PGD⁶; from 7% to 38%) again at severity 5. These findings confirm that DVD training renders models substantially more robust against adversarial attacks.

A Near-human-level robustness to Gaussian blur degradation



B Enhanced robustness to various image degradations



C Improved resilience to white-box and black-box adversarial attacks

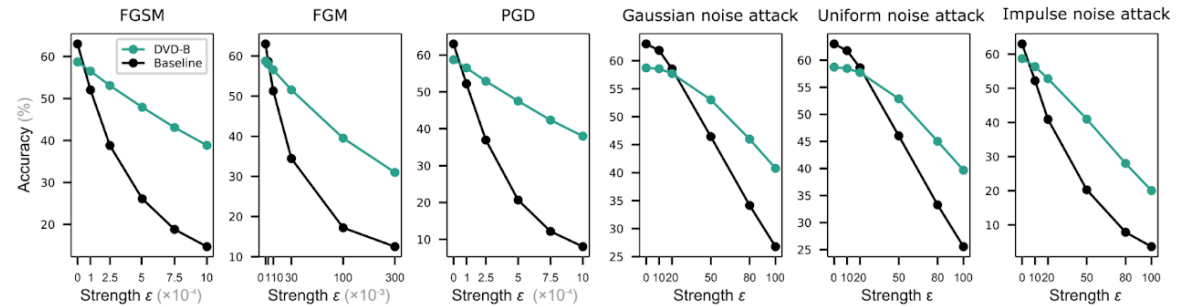


Figure 6 | ANNs trained with DVD exhibit enhanced degradation robustness to image degradations and adversarial attacks. A. Alignment of DVD-B-trained and baseline models with human response profiles under increasing severity of blurring for both face- and object recognition. **B.** Resilience to various image degradations, including different noises, blurring, weather, and image quality deficits for DVD-B-trained and baseline models. **C.** Robustness estimates of the DVD-B-trained model versus baseline under adversarial perturbations. White-box gradient-based attacks: Fast Gradient Sign Method (FGSM), Fast Gradient Method (FGM), and Projected Gradient Descent (PGD). Black-box attacks: L_2 -norm additive Gaussian noise, L_2 -norm additive uniform noise, and salt-and-pepper noise.

Discussion

Human-level robustness in vision has been a long-standing challenge for AI. Instead of “scaling up” data and architecture size, we here demonstrate that solutions can be found in biology. Across a range of experiments with different datasets and architectures, we show that exposing AI vision to the visual developmental trajectory of humans, from newborn to 25 years of age, yields significantly more robust, and human-aligned vision systems. DVD-trained models exhibit a new state of the art in shape-based decision making, outperforming large-scale AI foundation models and closing the gap to human behaviour^{16,24}. The same models also exhibited the ability to recognise abstract shapes hidden in complex backgrounds - again a test that large-scale foundation models fail⁸. In addition, DVD-training closely aligned our models with human psychophysical data upon gaussian image degradations and rendered them more robust to all other image perturbations tested⁹. Finally, DVD-trained models were shown to be more robust to a variety of black- and white-box adversarial attacks. Together, our analyses demonstrate that DVD-training yields models with a fundamentally different, robust feature set upon which they base their decisions. Rather than relying on distributed local features, such as textures, they derive their robustness from operating on integrative shape-based features.

Importantly, our models operate at rather low numbers of parametric complexity, compared to today’s large-scale MLLMs, and were demonstrated to rely on the extraction of shape information even when trained on small image datasets (e.g. mini-ecoset). This showcases that highly reliable vision models can be obtained outside of the industry’s tendencies for large-scale models and data - an important advance when considering the ecological footprint of today’s AI applications.

By running controlled rearing experiments, we report that the development of contrast sensitivity, rather than visual acuity or colour, played a pivotal role in obtaining shape-selective models. This runs counter to the intuitions behind previous studies that emphasised reduced visual acuity, simulated through image blurring¹⁰⁻¹³, as a key driver of shape bias. Yet, many promising aspects of biological vision remain to be explored for their implications on AI vision. Among many others, these include retinal preprocessing, overt visual information sampling, the differential roles of magno- and parvocellular pathways, and the co-development of different sensory modalities, the bodily action repertoire, and language abilities.

In addition to the benefits for machine vision, the current approach has implications for our understanding of how human vision may come to be so robust, indicating that “starting out poor” is an efficient way for the brain to learn highly robust visual features. As our experiments demonstrate, an early reliance on configural shape cues, enforced by missing high spatial frequency as well as overall frequencies with low power, may establish a perceptual bias that persists throughout human development, guiding human vision towards a shape-dominant visual processing strategy. Going forward, our models may serve as an important test-bed for deriving predictions on human visual developmental features, and provide a valuable starting point for explorations of the effects of medical interventions, such as the removal of congenital cataracts²⁵ and ways to mitigate the residual downsides of this intervention.

Methods

Neural network architectures and training

Developmental visual diet (DVD) preprocessing pipeline

DVD is implemented as a data preprocessing pipeline (Fig. 1A) that emulates the maturation of 3 visual aspects: visual acuity²⁶⁻⁴¹, chromatic sensitivity⁴²⁻⁴⁶, and contrast sensitivity⁴⁷⁻⁵². Quantitative psychophysical data from birth to 25 years (0-300 months) were collated and fitted with smooth, monotonic logistic functions (Fig. 1B, Fig. 1C, Fig. 1D); the resulting curves drive a data transformation schedule that spans the full training epochs.

Visual-Acuity simulation via Gaussian blur

Visual acuity is modelled by applying Gaussian blur (σ) to images, in accordance with measurable changes in Snellen-equivalent acuity (Fig. 1B). Following prior work on visual acuity simulation⁵², a 15° visual angle object viewed at 60cm allows a 20/20 observer to resolve ≈ 450 cycles, while a 20/600 observer can resolve only ≈ 15 cycles. For an image width of w pixels, we compute σ such that all spatial frequencies above $1/(w/15)$ are attenuated. Convolution with this filter produces an image approximating 20/600 acuity when $\sigma=4$ for an image size of 100×100 ⁵², which allows for converting any other Snellen fraction x into Gaussian blur σ :

$$\sigma(w, x) = \frac{4 \cdot x \cdot w}{(20/600) \cdot 100}$$

where w is the image width in pixels, and x is the Snellen visual acuity; increasing σ simulates reducing Snellen visual acuity.

Contrast sensitivity simulation via frequency-domain thresholding

Contrast sensitivity is modelled by applying an age-dependent amplitude threshold to each image's frequency-domain representation, selectively removing weak signal components that would be imperceptible to a developing human visual system. At each training epoch, the model is assigned an age t in months, and the corresponding image is processed to reflect contrast sensitivity limitations appropriate for that age. Specifically, we compute the image's discrete Fourier transform and extract the power spectrum across RGB channels. A dynamic amplitude threshold T_t was defined to suppress frequency components whose energy falls below the model's sensitivity at that age (see Fig. S3). This threshold is given by:

$$T_t = P_{\max} \cdot (1 - C_t) \cdot \max \left(\left\lfloor \frac{t}{\lambda} \right\rfloor, 1 \right)^{-1} \cdot \beta$$

where P_{\max} is the maximum spectral power across all RGB channels, C_t is the empirically estimated contrast sensitivity at age t normalized to the range $[0, 1]$, derived from quantitative human psychophysical data tracking contrast sensitivity from birth to early adulthood (0-300 months; see Fig. 1C). β and λ are fixed hyperparameters. β determines the base amplitude threshold in the frequency domain to map the initial contrast sensitivity in the spatial domain at birth, while λ controls the mapping between the rate of threshold decay in the frequency domain and the corresponding increase in contrast sensitivity over time in the spatial domain. Frequencies whose

amplitude falls below T_t are set to zero, effectively discarding fine-scale image information that would be undetectable at that stage of development. The resulting contrast-limited image is reconstructed by inverse Fourier transforming the filtered spectrum, yielding a naturalistic simulation of age-dependent visual experience for model training.

Chromatic sensitivity simulation via colour fidelity Interpolation

To model age-dependent changes in chromatic sensitivity, we applied a pixel-wise linear interpolation between grayscale and full-colour images, modulated by empirically derived chromatic sensitivity values ranging from 0% (newborn) to 100% (adult). These values represent the relative ability to perceive colour differences compared to mature observers. At each training epoch corresponding to developmental age t (in months), we define a chromatic sensitivity factor S_t in $[0, 1]$, fitted from behavioural and neurophysiological data (see Fig. 1D). This parameter governs the image transformation applied during training:

$$I_t = (1 - S_t) \cdot I_{\text{gray}} + S_t \cdot I_{\text{RGB}}$$

where I_{RGB} is the original full-colour image, I_{gray} is its grayscale (luminance-only) counterpart, and I_t is the resulting developmentally adjusted image at age t . This continuous schedule allows the model to experience a progressive increase in colour fidelity, mirroring the maturation of chromatic sensitivity over early development and into adulthood.

Hyperparameter tuning of DVD

The DVD preprocessing pipeline employs three key hyperparameters to control early visual experiences during model training: α (months per epoch), β (initial contrast threshold), and λ (contrast sensitivity mapping factor). For hyperparameter tuning, we swept α in $[1, 2, 4, 8]$, β in $[5e-5, 1e-4, 2e-4, 4e-4]$, and λ in $[50, 100, 150]$.

The parameter α defines the temporal resolution of the training process by mapping each training epoch to a specific number of developmental months. A smaller α results in finer temporal granularity, allowing the model to experience more gradual changes in visual input. A larger α accelerates progression through developmental stages. The parameter β sets the baseline for initial contrast sensitivity by defining the starting amplitude threshold in the frequency domain, simulating newborn vision. As training progresses, this threshold is lowered to reflect improving sensitivity. The parameter λ controls the rate at which the frequency-domain threshold decays over time, translating contrast sensitivity improvements in the spatial domain into reduced frequency-domain attenuation as development progresses.

Neural network architectures and training

We based our main experiments on the ResNet50 architecture as the default backbone for the baseline model and the DVD-trained models. The baseline models received conventional high-fidelity data preprocessing, whereas DVD-trained models were fed inputs transformed by the developmental visual-diet pipeline described below. We also trained a family of convolutional neural networks (CNNs) and vision transformer (ViTs) backbones (ResNet-50 by default; AlexNet, VGG-16, MobileNet-V2, ResNet-18, ResNet-101, ResNeXt-50, ViT-B/16 and DeiT-B/16¹⁸⁻²⁰ for generalisation tests across architecture; Fig.3B). All models were trained for 300 epochs, parallelized across two NVIDIA H100 GPUs using stochastic gradient descent (momentum = 0.9, weight decay = 1e-6,

learning rate = 1e-5), and received identical data augmentations including random horizontal flip, rotation, grayscale, brightness, Gaussian blur, sharpness, equalization and perspective.

Training datasets

We evaluated models trained with and without the DVD using three image datasets: mini-ecoset⁵³ (0.28 million images, 112 categories, including 12 added to match cue-conflict categories), ecoset¹³ (1.5 million images from 565 basic-level categories), and ImageNet-1K¹⁴ (~1.3 million images, 1,000 classes).

Model analyses

Shape vs texture bias

Shape bias is measured using cue-conflict stimuli, where texture and shape cues are in conflict¹. In accordance with Geirhos et al., we computed the shape-bias as:

$$B_{\text{shape}} = \frac{N_{\text{shape}}}{N_{\text{shape}} + N_{\text{texture}}}$$

where N_{shape} is the count of cue-conflict images correctly classified according to the shape cue, N_{texture} is the number classified according to the texture cue, and B_{shape} denotes the shape bias. This metric captures the proportion of shape-driven decisions when faced with conflicting shape-texture visual information. Unless otherwise specified, overall shape bias is reported as the median of category-level shape biases. N_{shape} is the count of cue-conflict images correctly classified according to the shape cue, N_{texture} is the number classified according to the texture cue, and B_{shape} denotes the shape bias. This metric captures the proportion of shape-driven decisions when faced with conflicting shape-texture visual information. Unless otherwise specified, overall shape bias is reported as the median of category-level shape biases.

Temporal dynamics of shape bias development

To track the emergence of shape bias throughout training, we saved weight checkpoints of both DVD-trained and baseline models at 5-epoch intervals. For each checkpoint, we computed shape bias and the corresponding shape/texture classification accuracy. Using the developmental clock parameter α (months per epoch), we can also translate these epochs into equivalent human developmental ages with the same visual acuity, contrast sensitivity, and chromatic sensitivity.

Controlled rearing studies

To disentangle the contributions of individual visual-development components, we conducted controlled-rearing experiments by training models with all possible combinations of three factors: visual acuity, contrast sensitivity, and chromatic sensitivity, resulting in seven distinct conditions: (1) all three present, (2) acuity+chromatic, (3) acuity+contrast, (4) contrast+chromatic, (5) acuity only, (6) chromatic only, and (7) contrast only. This systematic factorial design revealed that contrast sensitivity alone was sufficient to induce a significant shape bias, matching the performance observed in models trained with the full DVD pipeline.

Feature attribution

We applied Layer-Wise Relevance Propagation (LRP) to trace model predictions back through the network layers⁵⁴, assigning relevance scores to input pixels based on their contribution to the final

class decision. This allowed us to visualise whether models relied predominantly on shape-related or texture-related features when classifying cue-conflict images.

Image degradation robustness

We evaluated robustness to image degradation by measuring top-1 classification accuracy on objects and faces across 10 severity levels, and on 16 types of degradations, each tested at 5 severity levels. The degradations included noise (Gaussian noise, shot noise, impulse noise, speckle noise), blur (motion blur, zoom blur, Gaussian blur, defocus blur), weather effects (rain, icy window, drizzle, snow), and quality impairments (pixelate, JPEG compression, pixel dropout, wave distortion). Accuracy was recorded at each severity level to quantify the model's resilience under progressively challenging conditions across all degradation types.

Adversarial robustness

Adversarial robustness was quantified by measuring top-1 accuracy under both black-box²² and white-box attacks²³ at increasing intensity levels. Black-box attacks included: L₂-based Gaussian noise, uniform noise, and salt-and-pepper noise, each applied at perturbation amplitudes of 10, 20, 50, 80 and 100. White-box attacks comprised FGSM⁵ ($\epsilon=1e-4, 2.5e-4, 5e-4, 7.5e-4, 1e-3$), FGM⁵ ($\epsilon=1e-3, 1e-2, 3e-2, 1e-1, 3e-1$), and PGD⁶ ($\epsilon=1e-4, 2.5e-4, 5e-4, 7.5e-4, 1e-3$). Accuracy was recorded at each level to assess model stability under increasingly strong adversarial perturbations.

Abstract shape recognition

We evaluated abstract shape recognition using the IllusionBench dataset⁸, in which 16 distinct shape categories (airplane, bicycle, bird, bottle, car, cat, dog, dolphin, fork, guitar, mug, panda, paper_clip, sailboat, scooter, and teapot) are subtly embedded within 11 naturalistic scenes: bazaar market, city, medieval village, museum, time square, underwater ruins, cloud, forest, ocean, origami, and sand dune.

This benchmark tests a model's capability to detect global shape configurations embedded in natural scenes. We evaluate all models, vision-language models (VLMs) and standard vision models, using ImageNet-1K predictions mapped to 16 shape super-classes and 11 scene super-classes (same across models). Shape recall measures how often the predicted class belongs to the correct shape super-class. Scene recall measures how often the predicted class belongs to the correct scene super-class. For each dataset, recall is reported as the percentage of images where the correct shape or scene super-class was identified.

t-SNE embedding visualisation

To inspect the internal representations induced by DVD training, we extracted feature activations from the penultimate layer of each model (the last average-pooling layer for CNNs or the final pre-logit outputs for transformers) in response to the full IllusionBench dataset. These high-dimensional activation vectors were reduced to 50 principal components via PCA, a standard preprocessing step that stabilises t-SNE²¹ and mitigates noise. The reduced representations were then embedded into two dimensions using t-SNE with a perplexity of 30, PCA-based initialisation, and 1,000 iterations (random seed=42). The resulting 2D embeddings provide a clear visual summary of how models cluster stimuli based on learned feature similarity (Fig. 5C).

Code and data availability

All analyses of human and model data were performed in custom Python software, making use of PyTorch, numpy, and scikit-learn packages, among others. The code and data required to reproduce our results will be released on GitHub and OSF upon publication.

Acknowledgements

The authors acknowledge support by the European Research Council (ERC) StG grant 101039524 TIME (Kietzmann), ERC Consolidator grant ERC-CoG-2024101123101 (Cichy), CSC grant 202106120015 (Lu), and acknowledge that computations were in part supported by DFG-456666331.

Bibliography

1. Geirhos, R. *et al.* ImageNet-trained CNNs are biased towards texture; increasing shape bias improves accuracy and robustness. *ICLR* (2019).
2. Bowers, J. S. *et al.* Deep problems with neural network models of human vision. *Behav. Brain Sci.* **46**, e385 (2023).
3. Hermann, K., Chen, T. & Kornblith, S. The Origins and Prevalence of Texture Bias in Convolutional Neural Networks. in *Advances in Neural Information Processing Systems* vol. 33 19000–19015 (Curran Associates, Inc., 2020).
4. Hendrycks, D. & Dietterich, T. Benchmarking Neural Network Robustness to Common Corruptions and Perturbations. in (2018).
5. Goodfellow, I. J., Shlens, J. & Szegedy, C. Explaining and Harnessing Adversarial Examples. Preprint at <https://doi.org/10.48550/arXiv.1412.6572> (2015).
6. Madry, A., Makelov, A., Schmidt, L., Tsipras, D. & Vladu, A. Towards Deep Learning Models Resistant to Adversarial Attacks. in (2018).
7. Szegedy, C. *et al.* Intriguing properties of neural networks. in *2nd International Conference on Learning Representations, ICLR 2014* (2014).
8. Hemmat, A. *et al.* Hidden in Plain Sight: Evaluating Abstract Shape Recognition in Vision-Language Models. *NeurIPS* (2025).
9. Jang, H. & Tong, F. Convolutional neural networks trained with a developmental sequence of blurry to clear images reveal core differences between face and object processing. *J. Vis.* **21**, 6 (2021).
10. Jang, H. & Tong, F. Improved modeling of human vision by incorporating robustness to blur in convolutional neural networks. *Nat. Commun.* **15**, 1–14 (2024).
11. Yoshihara, S., Fukiage, T. & Nishida, S. Does training with blurred images bring convolutional neural networks closer to humans with respect to robust object recognition and internal representations? *Front. Psychol.* **14**, (2023).
12. Charles, W. & Leeds, D. Modeling Human Development: Effects of Blurred Vision on

- Category Learning in CNNs. (2020).
13. Mehrer, J., Spoerer, C. J., Jones, E. C., Kriegeskorte, N. & Kietzmann, T. C. An ecologically motivated image dataset for deep learning yields better models of human vision. *Proc. Natl. Acad. Sci.* **118**, e2011417118 (2021).
 14. Deng, J. *et al.* ImageNet: A Large-Scale Hierarchical Image Database.
 15. Huber, L. S., Geirhos, R. & Wichmann, F. A. The developmental trajectory of object recognition robustness: Children are like small adults but unlike big deep neural networks. *J. Vis.* **23**, 4 (2023).
 16. Dehghani, M. *et al.* Scaling Vision Transformers to 22 Billion Parameters. Preprint at <http://arxiv.org/abs/2302.05442> (2023).
 17. He, K., Zhang, X., Ren, S. & Sun, J. Deep Residual Learning for Image Recognition. in *2016 IEEE Conference on Computer Vision and Pattern Recognition (CVPR) 770–778* (IEEE, Las Vegas, NV, USA, 2016). doi:10.1109/CVPR.2016.90.
 18. Vaswani, A. *et al.* Attention is All you Need. in *Advances in Neural Information Processing Systems* vol. 30 (Curran Associates, Inc., 2017).
 19. Touvron, H. *et al.* Training data-efficient image transformers & distillation through attention. Preprint at <https://doi.org/10.48550/arXiv.2012.12877> (2021).
 20. Yee, M. N., Jones, S. S. & Smith, L. B. Changes in Visual Object Recognition Precede the Shape Bias in Early Noun Learning. *Front. Psychol.* **3**, (2012).
 21. Maaten, L. van der & Hinton, G. Visualizing Data using t-SNE. *J. Mach. Learn. Res.* **9**, 2579–2605 (2008).
 22. Rauber, J., Brendel, W. & Bethge, M. Foolbox: A Python toolbox to benchmark the robustness of machine learning models. Preprint at <https://doi.org/10.48550/arXiv.1707.04131> (2018).
 23. Nicolae, M.-I. *et al.* Adversarial Robustness Toolbox v1.0.0. Preprint at <https://doi.org/10.48550/arXiv.1807.01069> (2019).
 24. Gavrikov, P. *et al.* Can We Talk Models Into Seeing the World Differently? in *ICLR* (2025).
 25. Bouvrie, J. V. & Sinha, P. Visual object concept discovery: Observations in congenitally

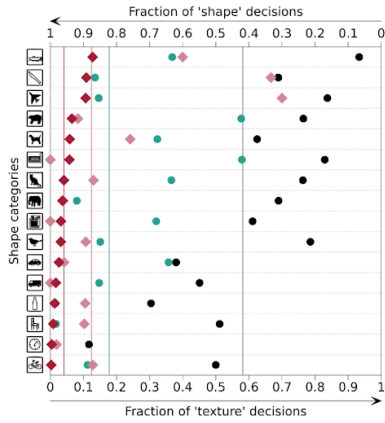
- blind children, and a computational approach. *Neurocomputing* **70**, 2218–2233 (2007).
26. Braddick, O. & Atkinson, J. Development of human visual function. *Vision Res.* **51**, 1588–1609 (2011).
 27. Caltrider, D., Gupta, A. & Tripathy, K. Evaluation of Visual Acuity. in *StatPearls* (StatPearls Publishing, Treasure Island (FL), 2024).
 28. Dobson, V., Clifford-Donaldson, C. E., Green, T. K., Miller, J. M. & Harvey, E. M. Normative Monocular Visual Acuity for Early Treatment Diabetic Retinopathy Study Charts in Emmetropic Children 5 to 12 Years of Age. *Ophthalmology* **116**, 1397–1401 (2009).
 29. Drover, J. R. *et al.* Normative pediatric data for three tests of functional vision. *Can. J. Ophthalmol.* **52**, 198–202 (2017).
 30. Drover, J. R. *et al.* Normative pediatric visual acuity using single surrounded HOTV optotypes on the Electronic Visual Acuity Tester following the Amblyopia Treatment Study protocol. *J. Am. Assoc. Pediatr. Ophthalmol. Strabismus* **12**, 145–149 (2008).
 31. El-Gohary, A., Abuelela, M. & Eldin, A. Age norms for grating acuity and contrast sensitivity measured by Lea tests in the first three years of life. *Int. J. Ophthalmol.* **10**, 1150–1153 (2017).
 32. Gal Katzhendler, Katzhendler, G., Daphna Weinshall & Weinshall, D. Potential upside of high initial visual acuity. *Proc. Natl. Acad. Sci. U. S. A.* **116**, 18765–18766 (2019).
 33. Inal, A. *et al.* Comparison of visual acuity measurements via three different methods in preschool children: Lea symbols, crowded Lea symbols, Snellen E chart. *Int. Ophthalmol.* **38**, 1385–1391 (2018).
 34. Kugelberg, U. Visual acuity following treatment of bilateral congenital cataracts. *Doc. Ophthalmol.* **82**, 211–215 (1992).
 35. Leone, J. F., Mitchell, P., Kifley, A., Rose, K. A., & Sydney Childhood Eye Studies. Normative visual acuity in infants and preschool-aged children in Sydney. *Acta Ophthalmol. (Copenh.)* **92**, (2014).
 36. Morale, S. E. *et al.* Normative pediatric visual acuity using electronic early treatment for

- diabetic retinopathy protocol. *J. AAPOS Off. Publ. Am. Assoc. Pediatr. Ophthalmol. Strabismus* **25**, 172–175 (2021).
37. Nolan, J. M. *et al.* Enrichment of Macular Pigment Enhances Contrast Sensitivity in Subjects Free of Retinal Disease: Central Retinal Enrichment Supplementation Trials – Report 1. *Invest. Ophthalmol. Vis. Sci.* **57**, 3429–3439 (2016).
38. O'Connor, A. R. & Milling, A. Normative data for the redesigned Kay Pictures visual acuity test. *J. Am. Assoc. Pediatr. Ophthalmol. Strabismus* **24**, 242–244 (2020).
39. Pan, Y. *et al.* Visual Acuity Norms in Preschool Children: The Multi-Ethnic Pediatric Eye Disease Study. *Optom. Vis. Sci. Off. Publ. Am. Acad. Optom.* **86**, 607–612 (2009).
40. Sanker, N., Dhirani, S. & Bhakat, P. Comparison of visual acuity results in preschool children with lea symbols and bailey-lovie e chart. *Middle East Afr. J. Ophthalmol.* **20**, 345 (2013).
41. Skelton, A. E., Maule, J., & Franklin, A.. Infant color perception: Insight into perceptual development. *Child development perspectives*, 16(2), 90-95 (2022).
42. Thomasson, M. A. & Teller, D. Y. Infant color vision: sharp chromatic edges are not required for chromatic discrimination in 4-month-olds. *Vision Res.* **40**, 1051–1057 (2000).
43. Vogelsang, M. *et al.* Impact of early visual experience on later usage of color cues. *Science* **384**, 907–912 (2024).
44. Teller, D. Y. Spatial and temporal aspects of infant color vision. *Vision Res.* **38**, 3275–3282 (1998).
45. Knoblauch, K., Vital-Durand, F. & Barbur, J. L. Variation of chromatic sensitivity across the life span. *Vision Res.* **41**, 23–36 (2001).
46. Brown, A. M., Lindsey, D. T., Cammenga, J. G., Giannone, P. J. & Stenger, M. R. The Contrast Sensitivity of the Newborn Human Infant. *Invest. Ophthalmol. Vis. Sci.* **56**, 625–632 (2015).
47. Dekker, T. M., Farahbakhsh, M., Atkinson, J., Braddick, O. J. & Jones, P. R. Development of the spatial contrast sensitivity function (CSF) during childhood: Analysis of previous findings and new psychophysical data. *J. Vis.* **20**, 4 (2020).

48. Norcia, A. M., Tyler, C. W. & Hamer, R. D. Development of contrast sensitivity in the human infant. *Vision Res.* **30**, 1475–1486 (1990).
49. Owsley, C., Sekuler, R. & Siemsen, D. Contrast sensitivity throughout adulthood. *Vision Res.* **23**, 689–699 (1983).
50. Pateras, E. & Karioti, M. Contrast Sensitivity Studies and Test- A Review. *Int. J. Ophthalmol. Clin. Res.* **7**, (2020).
51. Stavros, K. A. & Kiorpes, L. Behavioral measurement of temporal contrast sensitivity development in macaque monkeys (*Macaca nemestrina*). *Vision Res.* **48**, 1335–1344 (2008).
52. Vogelsang, L. *et al.* Potential downside of high initial visual acuity. *Proc. Natl. Acad. Sci.* **115**, 11333–11338 (2018).
53. Thorat, S., Doerig, A. & Kietzmann, T. C. Characterising representation dynamics in recurrent neural networks for object recognition. Preprint at <https://doi.org/10.48550/arXiv.2308.12435> (2023).
54. Bach, Sebastian, *et al.* On pixel-wise explanations for non-linear classifier decisions by layer-wise relevance propagation. *PloS one*, 10.7 (2015).

Supplementary Figures

A Shape bias across categories



B Examples

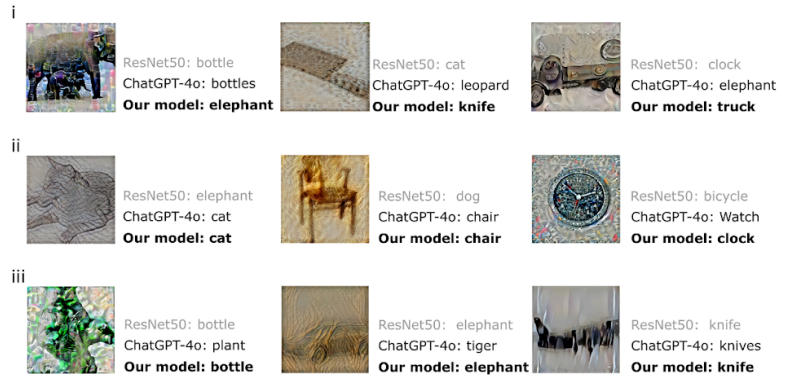


Figure S1 | Category-specific shape bias and prediction examples. **A.** Category-wise analysis of shape bias in DVD-B (green) compared to humans (ages 4-6 and adult; pink and red) and the ResNet-50 baseline (black). **B.** Example predictions from different models on cue-conflict stimuli. Row 1: Only DVD-B makes shape-biased predictions, while both the baseline ResNet50 model and ChatGPT 4o make texture-biased predictions. Row 2: Both DVD-B and ChatGPT 4o generate shape-biased predictions, while only the baseline model is texture-biased. Row 3: Challenging stimuli where all models make texture-based predictions.

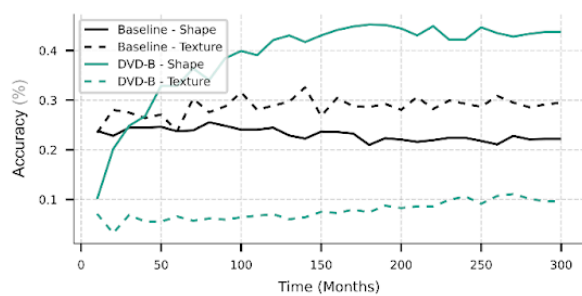
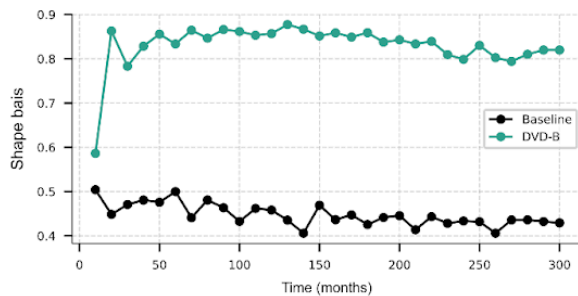


Figure S2 | Evolving shape bias over development. *Left:* Evolving shape bias of DVD-B model from newborn to 25 years old (300 months, 2 months per epoch for DVD-B, shown at 10-months/5-epochs resolution), strong shape bias emerges very early (0.87) by 20 months and gets maintained, in line with psychophysical evidence that babies are already shape biased at 2 years of age. *Right:* Percentage of shape-texture choices (correct predictions on shape/texture) across model training.

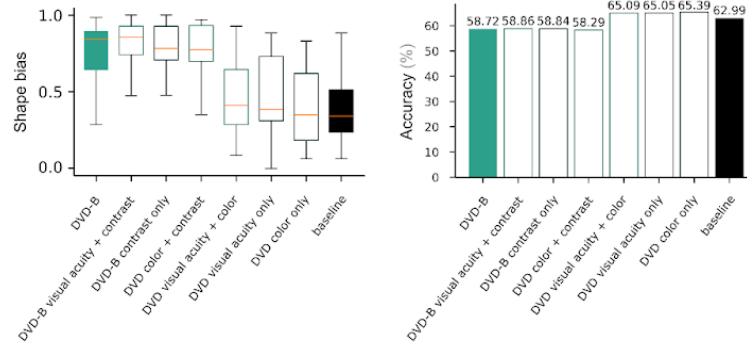


Figure S3 | Controlled rearing to study the role of different visual aspects in development (example: DVD-B). *Left: Shape bias for all controlled-rearing settings, emphasising contrast development. Right: Recognition performance of the controlled-rearing models.*

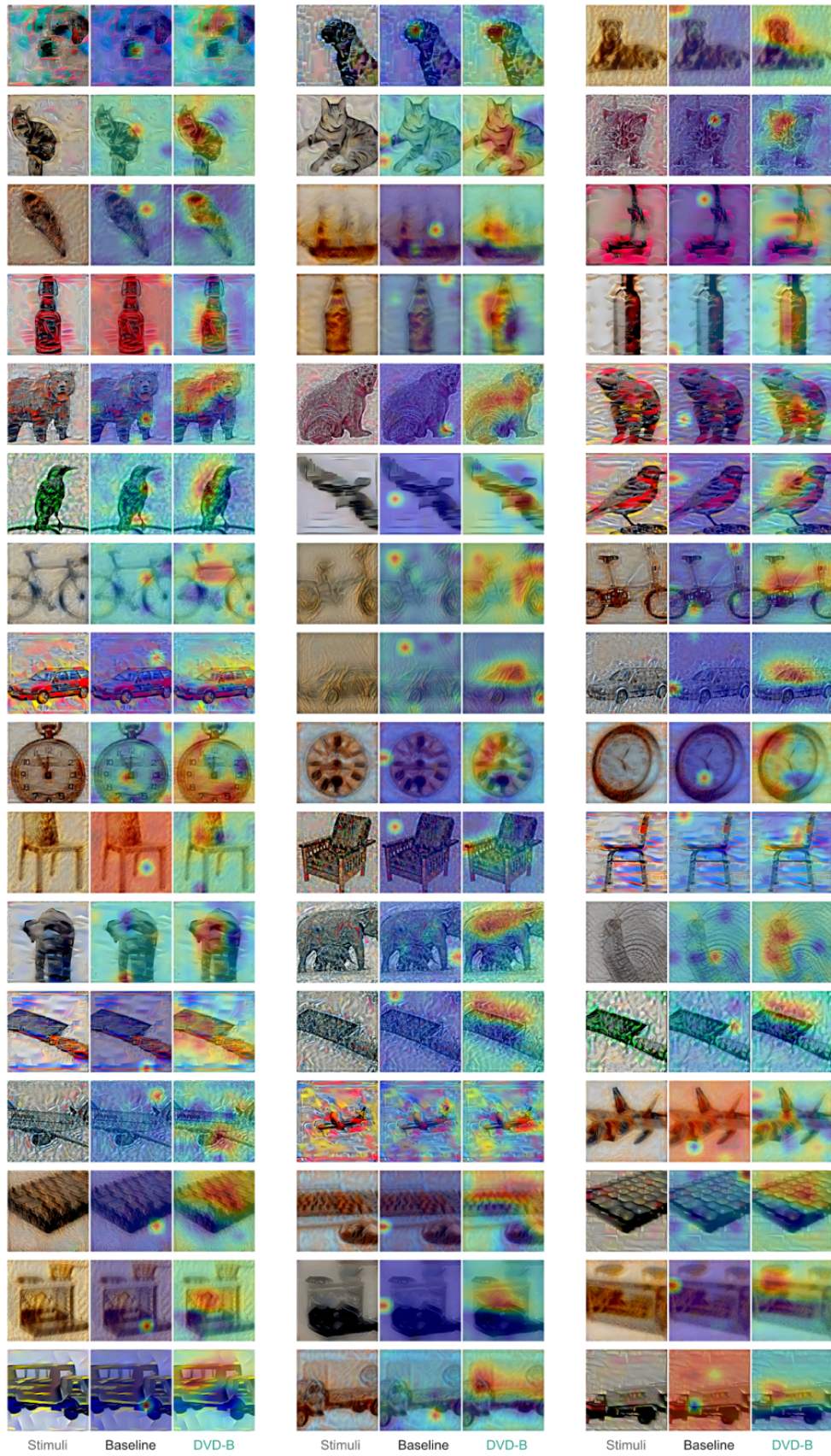


Figure S4 | Feature importance visualisation using layer-wise relevance propagation. *Further examples to visualise the generality of effects.*

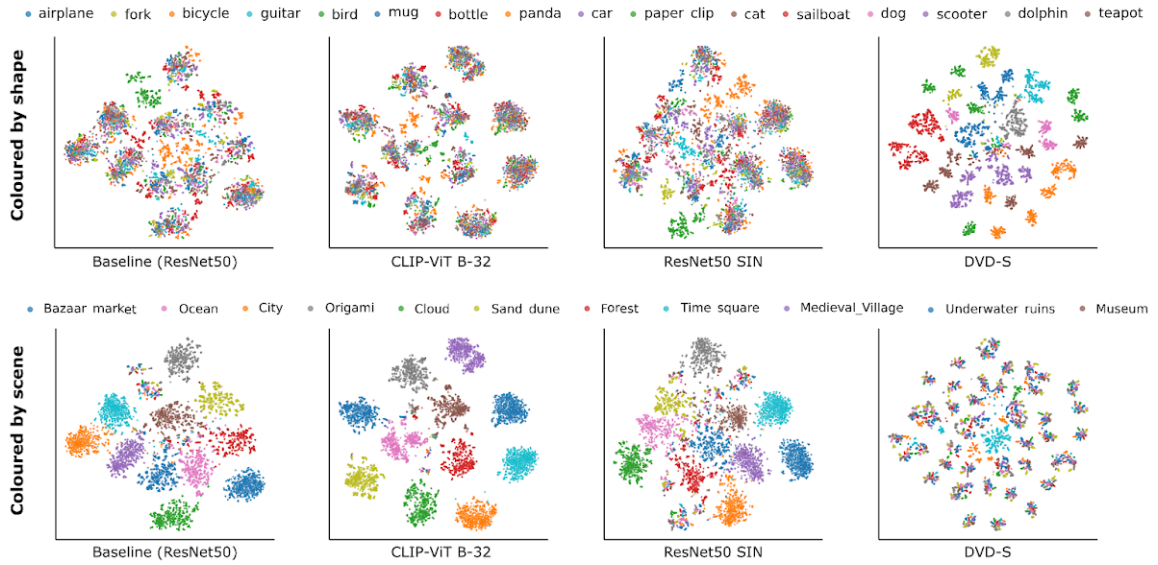


Figure S5 | t-SNE visualisation distinguishing abstract shapes from scenes. *t-SNE embeddings of IllusionBench images illustrate distinct clustering behaviour of abstract shapes under scene contexts for baseline ResNet50, CLIP-ViT B-32, ResNet50 with style-transfer training, and DVD-trained models (DVD-S model shown as example). Only DVD-trained models cluster images according to their abstract shape categories, whereas other models predominantly cluster images based on their scene contexts.*